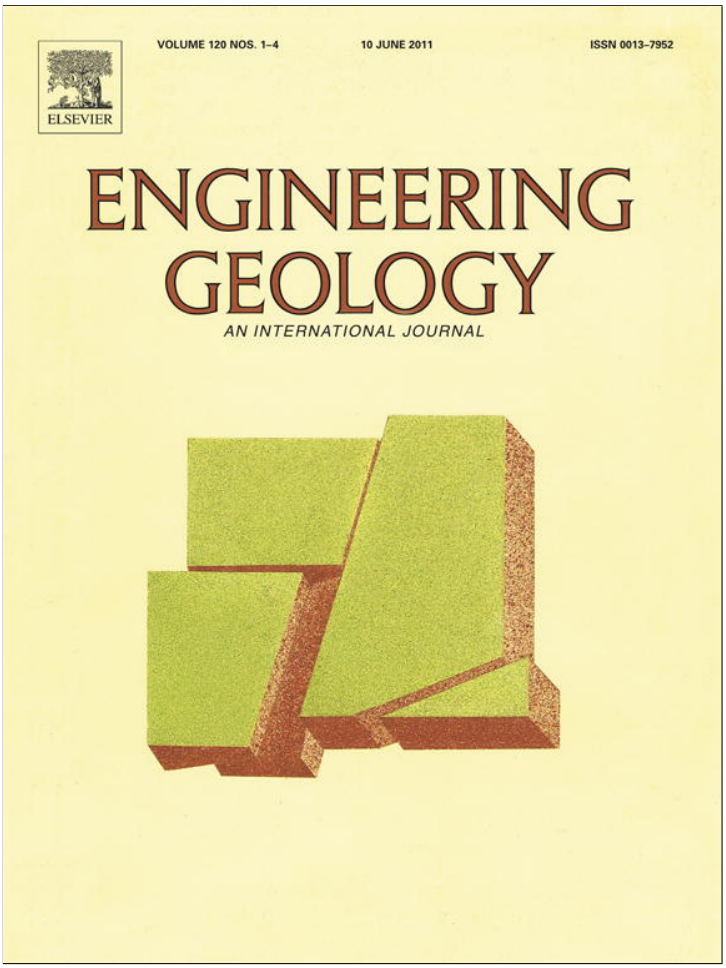

Engineering Geology 120 (2011) 18–31

Contents lists available at ScienceDirect

Engineering Geology

journal homepage: www.elsevier.com/locate/enggeo

Deep geophysical investigation of the large Séchilienne landslide (Western Alps, France) and calibration with geological data

Olivier Le Roux [a,b,e,*], Denis Jongmans [a], Johan Kasperski [c], Stéphane Schwartz [a], Pierre Potherat [c], Vincent Lebrouc [a], Richard Lagabrielle [d], Ombeline Meric [e]

[a] ISTerre (CNRS, UMR 5275), Observatoire des Sciences de l'Univers, Université Joseph Fourier, BP 53, F-38041, Grenoble cedex 09, France
[b] Institut EGID-Bordeaux 3, Equipe d'accueil Géoressources et Environnement (EA 4134), Université Michel de Montaigne, 1 allée Daguin, F-33607 Pessac cedex, France
[c] Centre d'Etudes Techniques de l'Equipement, Laboratoire de Lyon, 25 avenue François Mitterrand, Case n°1, F-69674 Bron cedex, France
[d] Laboratoire Central des Ponts et Chaussées, Centre de Nantes, F-44341 Bougenais, France
[e] Association pour le Développement des Recherches sur les Glissements de Terrain, 2 rue de la Condamine, Z.I. de Mayencin, BP 17, F-38610 Gières, France

ARTICLE INFO

Article history:
Received 12 November 2010
Received in revised form 10 March 2011
Accepted 12 March 2011
Available online 23 March 2011

Keywords:
Séchilienne landslide
Structural study
Seismic tomography
Electrical resistivity tomography
Porosity
Landslide volume

ABSTRACT

A geophysical imaging campaign, including four 950 m electrical profiles and four 470 m long seismic profiles, was performed on the large Séchilienne landslide with the objective of constraining the depth and the volume of the affected zone. Compared to the undisturbed ground, the moving area exhibits lower velocity and higher resistivity values. Comparison with existing geodetic, geomorphic and geological data (investigation gallery and borehole) allowed showing that these geophysical parameter variations result from intense fracturing and the progressive development of air-filled voids within the moving mass. A maximum thickness of 150 m to 200 m was found in the most deconsolidated zones. Locally, near-vertical very low resistivity anomalies were evidenced, related to cataclasis zones filled with clayey material. Applying the Wyllie's experimental law, rock mass porosity images were derived from seismic tomography profiles. Porosity between 30% and 4% was found from the top to the bottom of the deconsolidated zone, explaining the deep water table. Considering a porosity threshold of 3.7% for the sound bedrock, the total volume of the Séchilienne landslide was estimated to about $60 \pm 10 \times 10^6 m^3$, a more precise bracket than the previous estimations (20×10^6 to $100 \times 10^6 m^3$).

1. Introduction

Since the last deglaciation, in the mountainous domain, the slope evolution has been partly controlled by deep-seated gravitational slope deformations (DSGSD) (Ballantyne, 2002), which are characterized by a large-scale destabilized volume, a long-time evolution and diffuse deformation without clear slip surface (Agliardi et al., 2001; Brückl and Parotidis, 2005; Petley et al., 2005). DSGSD were observed in all mountain belts, for various lithological contexts (Dramis and Sorriso-Valvo, 1994; Agliardi et al., 2001) and inducing catastrophic landslides at a smaller scale (Brückl and Parotidis, 2005; Chemanda et al., 2005; Bachmann et al., 2009). Recent studies have shown that the present-day active gravitational movements are often nested in a larger deformed zone (Agliardi et al., 2001; Brückl and Parotidis, 2005; Petley et al., 2005; Bachmann et al., 2009). The slope failure initiation mechanism, the affected volume and the evolution of gravitational deformation are still open and debated questions (e.g. Le Roux et al., 2009; Guglielmi and Cappa, 2010; Sanchez et al., 2010). The surface affected by active gravitational movement can be well delimited using geodetic and/or remote sensing measurement (e.g. Duranthon et al., 2003; Metternicht et al., 2005; Delacourt et al., 2007). On the contrary, at larger scale, the volume affected by the gravitational destabilization is often poorly constrained.

In a rock mass, electrical resistivity and seismic velocity can vary with the nature of the geological formation, the fracturing and weathering degree as well as with the presence of water (Telford et al., 1990; Reynolds, 1997). In the last two decades, geophysical prospecting methods have become a major tool to investigate the internal structure of landslides (for a review, see Jongmans and Garambois, 2007). Gravitational deformations usually modify the mechanical and hydrogeological ground characteristics, which in turn affect the measured geophysical parameters that can be used to map the landslide body. In rocks, seismic properties like P and S wave velocities (Vp and Vs) have been shown to be highly sensitive to fracturing and are extensively used for characterizing the rock quality (Leucci and De Giorgi, 2006; Barton, 2007). Landslide-induced fracturing in rocks was mapped using P-wave tomography on the unstable mountain slope of Randa (Valais, Swiss Alps) and extremely low velocity values were found, resulting from the ubiquitous presence of dry cracks and fault zones (Heincke et al., 2006). Electrical resistivity (ρ) can also provide information about fracturing, which can generate an increase (Meric et al., 2005) or a decrease (Lebourg

* Corresponding author at: Institut EGID-Bordeaux 3, Equipe d'accueil Géoressources et Environnement (EA 4134), Université Michel de Montaigne, 1 allée Daguin, F-33607 Pessac cedex, France. Tel.: +33 557121013; fax: +33 557121001.
E-mail address: Olivier.LE_ROUX@egid.u-bordeaux3.fr (O. Le Roux).

0013-7952/$ – see front matter © 2011 Elsevier B.V. All rights reserved.
doi:10.1016/j.enggeo.2011.03.004

et al., 2005; Heincke et al., 2010) of the resistivity, in dry or saturated rocks, respectively.

This study aims at determining the thickness of the mass and the corresponding volume affected by the Séchilienne gravitational movement (Belledonne Massif, French Alps). Seven long geophysical profiles (3 of them are electrical and 4 are seismic) were performed in summer 2008 on the Sechilienne landslide. Geological information gathered at the surface and in a survey gallery helped interpreting the geophysical data. The landslide volume was estimated from the geophysical data using empirical laws with a rock porosity threshold.

2. Geological, geomorphological and kinematic settings

The Séchilienne landslide is located in the southwestern part of the Belledonne Massif (western Alps) (Figure 1). The massif, which extends over more than 120 km in an N30 direction with an altitude of 3000 m a.s.l., is bounded to the west by the large topographic depression of the Isère Valley (Figure 1b). The massif, one of the Palaeozoic External Crystalline Massifs of the French Alps, is part of the Hercynian orogen reworked during the Alpine orogenesis. These basement rocks consist of a complex of different metamorphic rocks (gneisses, amphibolites and micaschists, Figure 1c) (Ménot, 1988). The Belledonne massif is affected by a recurrent active deformation (Martinod et al., 2001; Thouvenot et al., 2003). The localization of the seismic sources, provided for more than 10 years by the Sismalp seismological network, shows a concentration of earthquakes along an axis parallel to the western edge of the massif (Thouvenot et al., 2003). This alignment of seismic events with M_L magnitudes lower than 3.5 and located at shallow depths (less than 10 km) extends on more than 50 km. This seismic activity restricted below the western limit of the Belledonne massif is suspected to reflect the tectonic activity of the so-called Belledonne Border Fault (BBF, Figure 1b and c)

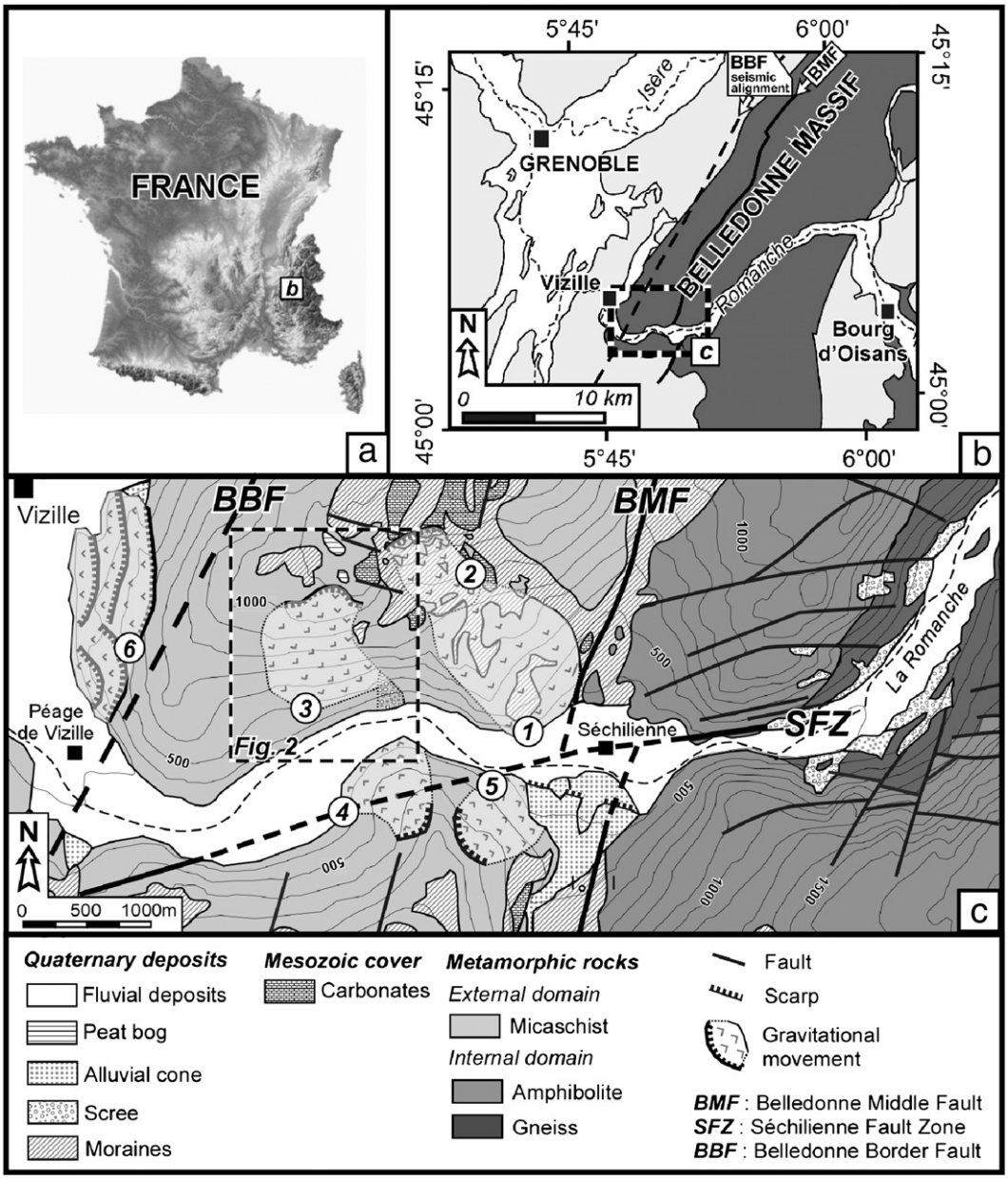

Fig. 1. (a) Location of the study area in France. (b) Structural map of the southwestern part of the Belledonne External Crystalline Massif centered on the lower Romanche Valley. The location of the Belledonne Border Fault (BBF) seismic alignment is inferred from Thouvenot et al. (2003). (c) Geological and structural map of the lower Romanche valley (modified from Barféty et al., 1972). Rock mass movements are labeled from 1 to 6. The Séchilienne landslide is number 3. The rectangle in dashed line locates Fig. 2.

(Thouvenot et al., 2003). However, this structure has never been observed at the surface through geological or morphological features (Le Roux, 2009).

The massif is divided into two major tectonic and lithological domains, the external domain to the west and the internal one to the east (Guillot et al., 2010). These two blocks are separated by a major Late Paleozoic near-vertical fault so-called Belledonne Middle Fault (BMF) (Figure 1c). The external domain, which is carved by the east–west trending lower Romanche River (Figure 1), features micaschists unconformably covered with Mesozoic sediments and Quaternary deposits (Figures 1b and 2a). The valley morphology, resulting from the alternate activity of water and ice during Quaternary times (Montjuvent and Winistorfer, 1980; Le Roux, 2010), consists of a glacial plateau (1150 m a.s.l.) dominating steep slopes, around 35 to

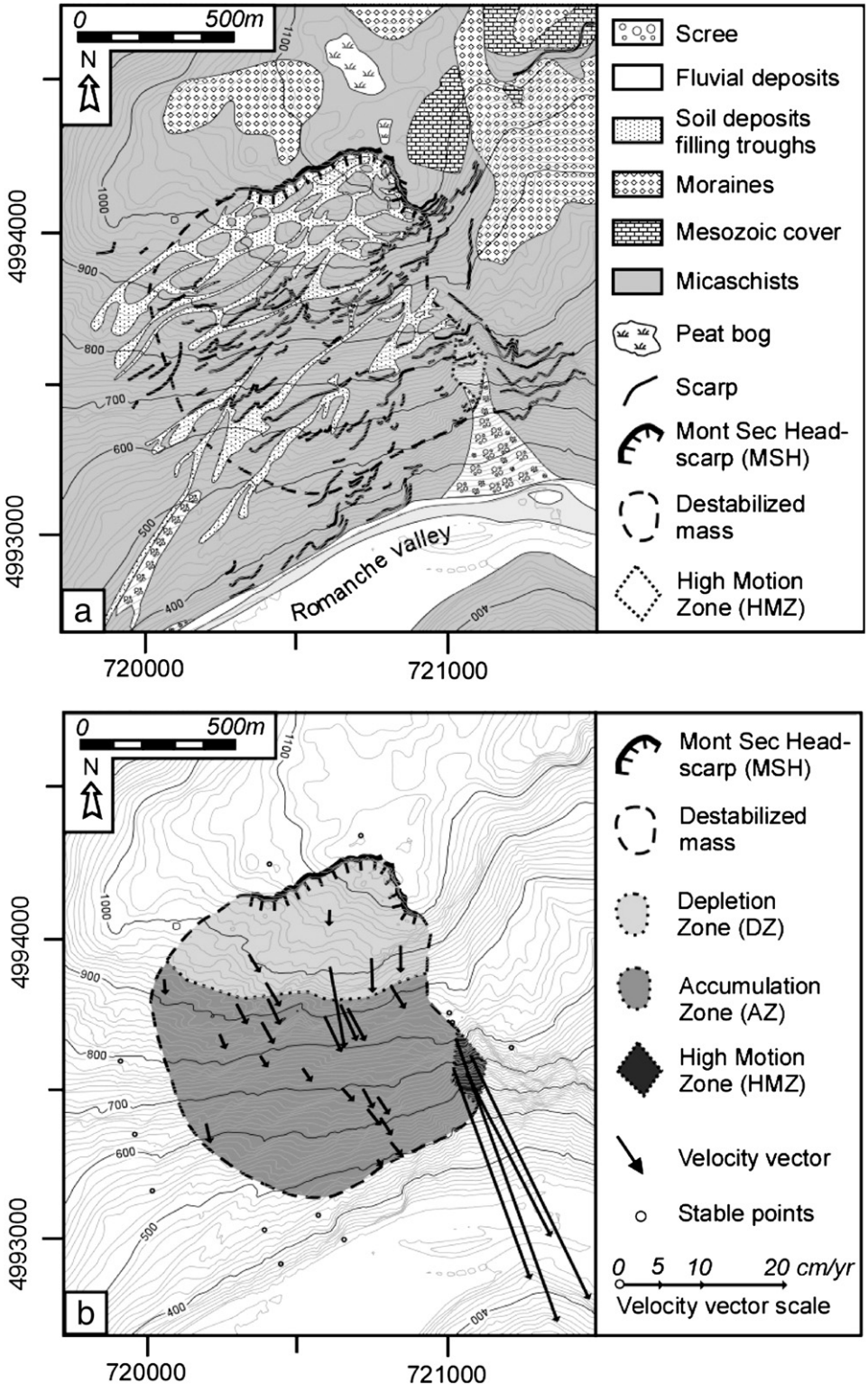

Fig. 2. (a) Geological and geomorphic structures of the Séchilienne landslide. (b) Kinematic map with the slide velocity vectors and the delineation of the accumulation, depletion and high motion Zones.

40°, which extends down to the Romanche river. This slope is affected by active or paleo large-scale rock mass movements between 450 and 1150 m elevation (Barféty et al., 1970) (Figure 1c).

The Séchilienne landslide is the most active gravitational movement at the present time in the area (Figure 2) (Duranthon et al., 2003). To the north, it is delineated by a major head scarp (Mont Sec Head-scarp, MSH), several hundred meters wide and several tens of meters high, and to the east by a lateral scarp whose position is controlled by north–south oriented fault. Below the head scarp, a low-slope depletion zone (DZ) between 1100 and 950 m a.s.l. exhibits a series of large depressions and salient blocks (Figure 2). The lower part of the landslide, between 950 and 450 m a.s.l., shows steep convex slopes (> 40°, Figure 2) interpreted as an accumulation zone (AZ) (Vengeon, 1998). The western and lower limits of the landslide cannot be easily traced in the morphology.

The mechanism usually suggested for the Séchilienne landslide triggering is the slope unloading and debutressing resulting from the late Würmian Romanche Glacier melting (15,000 years BP) (Vengeon et al., 1999; Potherat and Alfonsi, 2001). However, recent cosmic ray exposure data acquired along the Séchilienne head scarp (Le Roux et al., 2009) indicated that the slope failure occurred at 6.4 ± 4 ^{10}Be ka, more than 5400 years after the total deglaciation of the valley. The Sechilienne landslide then does not appear as an immediate consequence of debutressing in the Romanche valley.

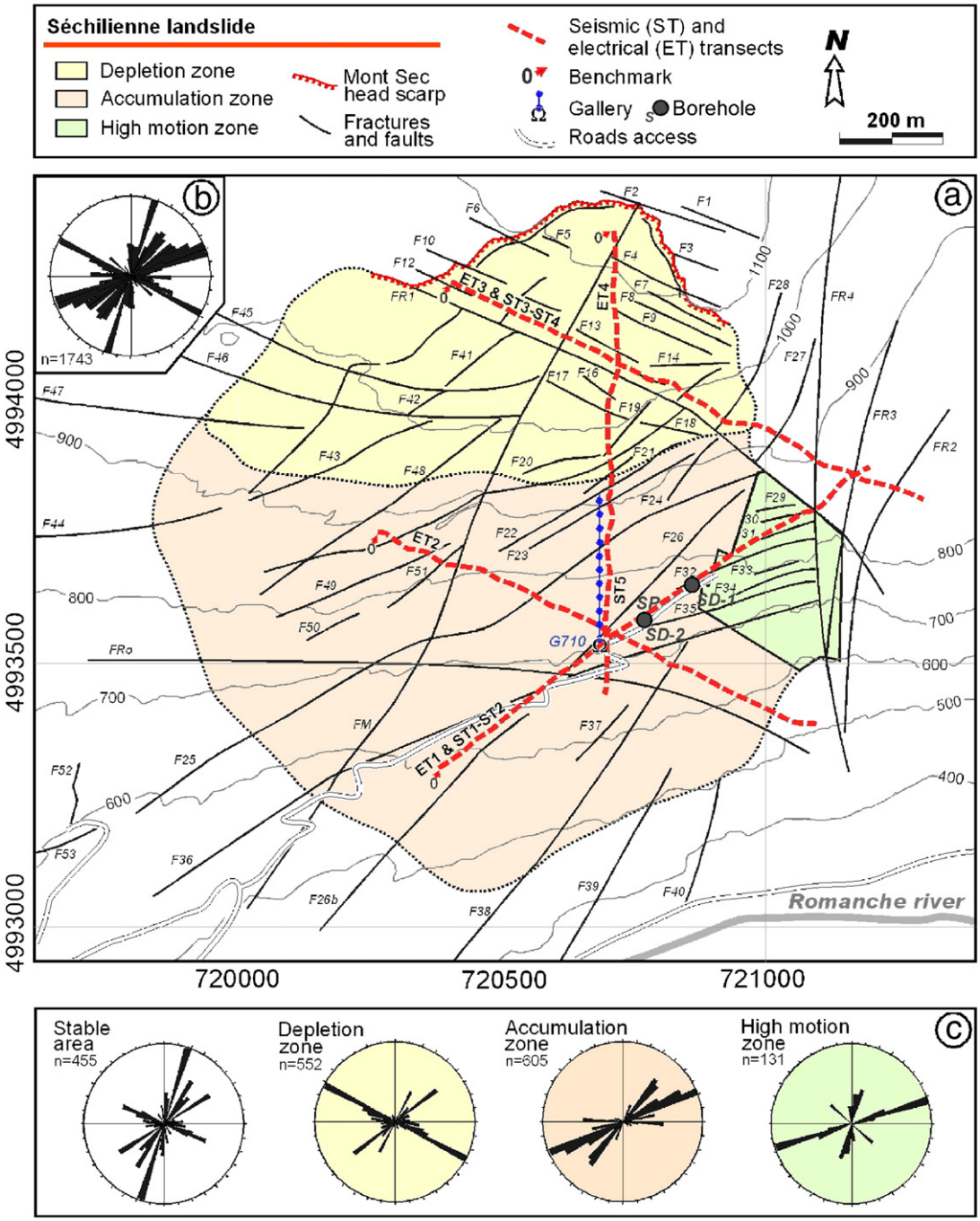

Fig. 3. (a) Structural sketch map of the Séchilienne slope (modified after Potherat and Alfonsi, 2001). The depletion, accumulation, high motion and stable zones are in yellow, pink, green and white, respectively. The 240 m long gallery is labeled G710. The location of the three boreholes is indicated by gray circles. (b) Rose diagram of structural data for the Séchilienne slope. (c) Rose diagrams (see text for detail) for the four morphological zones. The location of the electrical tomography profiles (labeled ET1 to ET4) and of the seismic tomography profiles (labeled ST1 to ST5) is given.

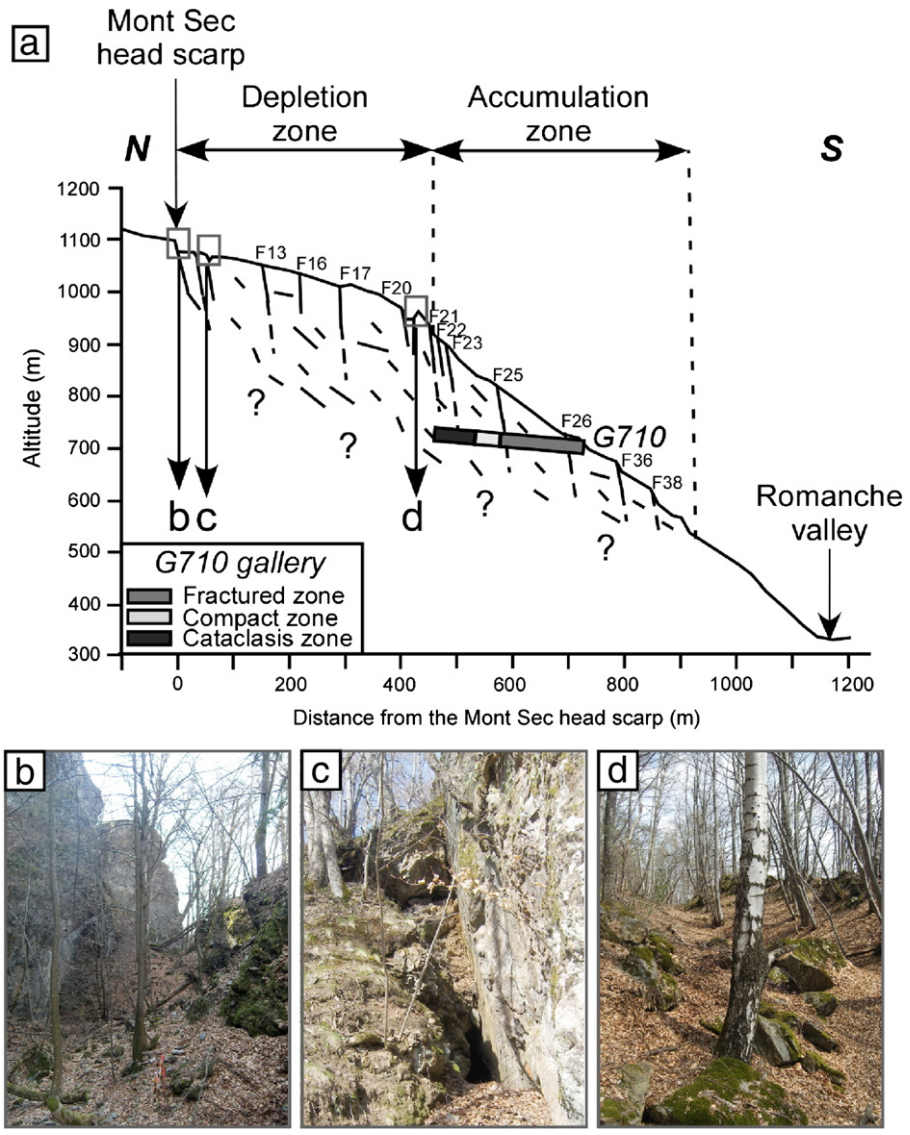

Fig. 4. (a) North–south cross section along profile ET4 (see location in Fig. 3) with the main fractures observed at the surface and the fracturing zones depicted into the G710 gallery (redrawn from Vengeon et al., 1999) (b) Photography of the Mont Sec head scarp. (c) Photography of a V-shaped through located downslope from the Mont Sec head scarp. (d) Photography of the major through delineating the depletion zone to the north from the accumulation zone to the south. All pictures are taken from the west and their location is given in Fig. 4a.

Since the 1980s, a monitoring system (extensometers, geodetic measurements, tacheometers and microwave radar) has been progressively installed by the *Centre d'Etudes Techniques de l'Equipement* (CETE) of Lyon (Evrard et al., 1990; Vengeon et al., 1999; Duranthon et al., 2003). Monitoring results (Figure 2b) show relatively homogeneous orientations (N140) and inclinations (10 to 20°) of displacement vectors over the two destabilized areas described above, with relatively low displacement rates (2 to 15 cm/year) (Giraud et al., 1990;; Durville et al., 2004; Kasperski et al., 2010). To the west and to the south, those regularly decrease, allowing the landslide body to be approximately delineated (Figure 2b). However, to the east, a particularly active zone can be distinguished in the lower part of the landslide. This high motion zone (HMZ), whose volume has been estimated to about $3\times10^6 m^3$ (Durville et al., 2004), exhibits high sliding velocity vectors reaching a maximum of 150 cm/year (Figure 2b). This frontal movement generates frequent rock falls. The displacement rate series in this zone displayed seasonal variations, with an increase by a factor of three during heavy rainfall and snow melting periods in winter and spring (Rochet et al., 1994;; Alfonsi, 1997; Vengeon, 1998; Durville et al., 2004). After 2006, this seasonal influence disappeared, associated with an increase in displacement rate (Kasperski et al., 2010). Several investigation campaigns have been performed in the last fifteen years. In 1993–1994, a 240 m long survey gallery (G710 in Figure 3a) was excavated at 710 m a.s.l., revealing a succession of rigid moving blocks delimited by highly fractured zones (Vengeon, 1998). This gallery did not reach the sound bedrock and did not answer the question of the existence of a deep rupture surface. A hydrochemical survey was conducted on the landslide (Vengeon, 1998; Guglielmi et al., 2002). Results suggested the

Fig. 5. Seismic refraction tomography sections with initial model inferred from plus–minus method interpretation. (a) Profile ST1–ST2, 10 iterations, RMS = 1.0%. Borehole SD-1 is located with the limit of detected movements by inclinometer measurements (horizontal line). (b) Profile ST3–ST4, 10 iterations, RMS = 1.2%. (c) Profile ST5, 10 iterations, RMS = 1.7%. (Meric et al., 2005). White cross-hatching: low ray coverage area. SZ: Stable Zone. HMZ: High Motion Zone. MSH: Mont Sec Head scarp. DZ: Depletion Zone. AZ: Accumulation Zone. G710: survey gallery.

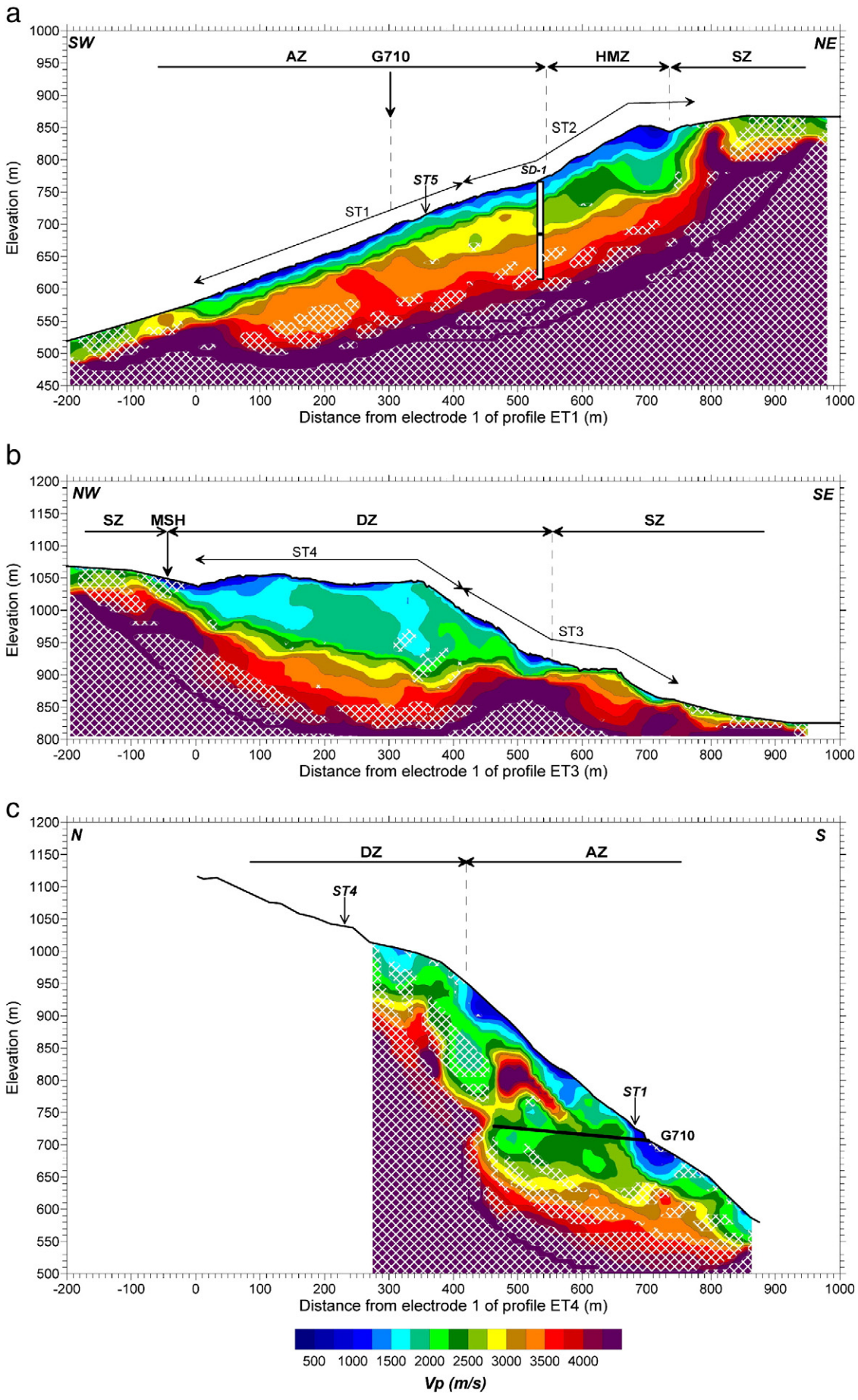

existence of a deep phreatic zone extending into the fractured metamorphic bedrock, with a probable 100 m thick vadose zone above. With intensive rainfall and long-term water recharge (> 45 days), this vadose zone could be saturated during rainy periods, increasing the displacement rate (Vengeon, 1998). Recently, Meric et al. (2005) performed a geophysical survey on the Séchilienne landslide, which showed that the moving zone is identified by higher resistivities and lower P-wave velocities, compared to the stable area. They interpreted these results as the consequence of a high fracturing in dry micaschists. Combination of morphological features, displacement rate values and geophysical measurements allowed the moving mass to be delineated at the surface (Figure 2). The area affected by the landslide has been estimated to about $1\times10^6\,m^2$ (Le Roux, 2009). On the contrary, the depth of the sound bedrock was still poorly controlled, which made the total landslide volume assessment uncertain. Recently, three 150 m-depth boreholes were drilled between the high-motion zone and the G710 gallery (Kasperski et al., 2010). Two of the boreholes were equipped with inclinometer casing (SD-1 and SD-2, Figure 3a). For SD-1, monthly measurements between February and July 2010 indicate horizontal displacements from the surface to 80 m depth. Piezometric measurements made in the third borehole (SP, Figure 3a) showed that the water level is deep (below 130 m depth).

3. Methods

3.1. Structural analysis

Based on field work surveys, aerial photo interpretation and inner-rock information collected in exploration galleries, a structural sketch map showing the main detected fractures (or faults) at the scale of the Séchilienne slope was proposed by Potherat and Alfonsi (2001) (Figure 3a). For this study, the fracture orientation data have been statistically reprocessed and weighted as a function of their length. These lineament orientations are then reported in rose diagrams at the scale of the whole slope (Figure 3b) in order to determine the main fracture orientations. The dataset was also treated according to and for the four different morphological zones (stable area, depletion zone, accumulation zone and high motion zone) of the Séchilienne slope (Figure 3c). Fracturing data were also collected and spatially analyzed in a near horizontal 240 m long gallery driven in 1993–1994 at an altitude of 710 m a.s.l. (G710, Figure 3a).

3.2. Geophysical prospecting

Four 950 m long electrical tomography profiles (labeled ET1 to ET4, Figure 3a) and four 470 m long seismic profiles (labeled ST1 to ST4, Figure 3a) were conducted in the Séchilienne landslide.

Along each electrical profile, 96 electrodes 10 m apart were used with a Wenner–Schlumberger (for profiles ET1, ET3 and ET4) and Wenner (for profile ET2) arrays for their low noise sensitivity (Dahlin and Zhou, 2004). The ground surface being locally very resistive, the contact between soil and electrode were improved by adding bentonite clay mixed with salt water, allowing to transmit a minimal current of 20 mA through the ground. Four measurements were stacked for each pair of current and potential electrodes. Measurements with a standard deviation greater than 1% were eliminated of the pseudo-section. The numbers of remaining points were respectively 1698, 1254, 2028 and 2199 for profiles ET1, ET2, ET3 and ET4. Finally, a median filter was applied to the apparent resistivity data sets to remove the influence of outliers. Apparent resistivity data were then inverted using the Res2dinv software (Loke and Barker, 1996; Loke, 1998) with the L_1-norm to get an image of the resistivity distribution in the ground. This robust inversion method was chosen to image the expected sharp boundaries and to minimize the effect of error measurements (Claerbout and Muir, 1973; Loke, 1998). Due to the heterogeneity and the sharp vertical and horizontal variations of the data set, the initial damping factor, the vertical to horizontal flatness filter ratio and the number of nodes between adjacent electrodes were respectively fixed to 0.16, 1 and 4 (Loke, 1998). The inversion process was stopped after 5 iterations. The inversion stability and robustness were controlled by applying a median filter and adding a random noise of $\pm10\%$ to the measured apparent resistivity and by modifying the starting model.

Along each seismic profile, 20 explosive shots including 4 offset shots were recorded by 48 vertical receivers (4.5 Hz) 10 m apart. First arrival times were picked and processed using the plus–minus method (Hagendoorn, 1959). The obtained seismic models were then used as initial velocity sections for inverting the first arrival times, applying the SIRT method (Dines and Lyttle, 1979; Demanet, 2000) to get an image of the ground in P-wave velocity (Vp). ST1 and ST2 were inverted together, as well as ST3 and ST4. The inversion process was stopped after 10 iterations. The robustness and stability of all images were tested by starting with another initial model (homogeneous with a velocity of 4000 m/s) and by adding a random noise up to $\pm10\%$ on the first arrival times. Areas with poor resolution, i.e. low ray coverage, are superposed to the velocity section in order to determine the penetration depth of the seismic rays (white cross-hatching).

3.3. Porosity assessment

Geophysical methods only give indirect information — geophysical parameters — instead of geotechnical properties. Numerous mixture laws have been proposed to link *Vp* or ρ to the porosity Φ, mostly in saturated sedimentary rocks (Mavko et al., 1998). The geophysical properties of a mixture of grains and pores can be predicted knowing the volume fractions and the properties of the two phases, as well as the pore shape. For *Vp*, one of the simplest models is the empirical equation proposed by Wyllie et al. (1956) for fluid saturated rocks:

$$\frac{1}{Vp}=\frac{\Phi}{Vp_f}+\frac{1-\Phi}{Vp_m} \tag{1}$$

where *Vp*, Vp_f and Vp_m are the P-wave velocities of the saturated rock, of the pore fluid and of the mineral material composing the rock, respectively. This empirical relation, which hypotheses that the travel time is the sum of the transit time in the mineral material and the transit time in the pore fluid, cannot be justified theoretically and should be limited to isotropic, consolidated and fluid saturated rocks at high enough effective pressure (Mavko et al., 1998). According to these authors, this equation can however be used to estimate the porosity from measurements of seismic velocity and knowledge of the rock type and pore-fluid content. In the case of fractures in dry rocks, Vp_f is the air velocity and Φ is the fissure porosity. Although the isotropy and high effective pressure conditions are not fulfilled in such a shallow metamorphic rock, the Wyllie's law was applied with a rock porosity threshold in order to grossly estimate the thickness of the mass affected by the landslide activity from the seismic tomographies.

The landslide volume was then estimated by interpolation between the three seismic images, one previous Vp profile (Meric et al., 2005) and the landslide lateral limits. We used the Surfer software to reconstruct the landslide geometry, applying the Natural Neighbor gridding method (Watson and Philip, 1987). The advantage of this technique is that it does not extrapolate contours beyond the convex hull of the data locations. The uncertainty of the landslide volume was estimated by applying other interpolation methods and porosity threshold.

4. Analysis of the landslide fracturing

Fig. 3a presents the structural sketch map of the Séchilienne landslide determined by Potherat and Alfonsi (2001). At the scale of the slope (Figure 3b), 3 main fracture orientations have been evidenced: N20 to N30, N70 and N110 to N140. The first set, which is major in the stable

zone, includes the N20–N30 near-vertical faults (e.g. FM, FR2, FR3 in Figure 3a) that are near-parallel to the main Palaeozoic Belledonne Middle Fault. Their orientation fits with the main foliation plane measured over the slope. The N70 set (F20 to F23, F29 to F36 in Figure 3a) corresponds to a major regional fracture family evidenced on both sides of the BMF, as well as in the micaschists as in the amphibolites (Le Roux et al., 2010) and is probably inherited from the regional tectonics (Figure 1b). In the high motion and accumulation zones where this set is dominant (Figure 3c), the N70 trending fractures are open and delineate near vertical slabs toppling downslope. These open fractures have been progressively filled with coarse scree deposits and now appear as V-shaped troughs of various widths and depths (Figure 4). In the high motion zone, toppling is very active and generates the numerous recorded rockfalls (Helmstetter and Garambois, 2010). The N70 trending fractures then turned out to play a major role in the gravitational deformation in the accumulation and active zones and most of the displacement vectors measured in the two zones (Figure 2) are perpendicular to the fracture trend. In the lower part of the Séchilienne slope the fracture orientation evolves from N70 to N50 (F35 to F40 in Figure 3a). Finally, the third fracture orientation, N110 to N140 (F1 to F18, FR1 in Figure 3a), is dominant in the depletion zone (Figure 3c). This fracture family is an inherited tectonic structure also observed at the regional scale by Le Roux et al. (2010).

The north–south oriented gallery (G710, Figure 3a) crosses the near vertical foliation whose orientation varies from N170 to N20. Displacement measurements performed in the gallery showed that this latter did not reach the sound bedrock (Vengeon, 1998). Fracturing is highly heterogeneous along the gallery and three zones can be distinguished (Figure 4, Vengeon, 1998). From 0 to 140 m, the rock is intensively fractured and exhibits three sets of locally open fractures: a first family of near-vertical fractures oriented N90 to N135–150, a second set running N80/50°N and a third set oriented N75, dipping 50°S near-parallel to the slope. From 140 to 170 m, the rock is little fractured and constitutes a compact block. Beyond 170 m, the gallery crosses a succession of compact blocks and crushed zones (cataclasis). These meter-to-decameter thick zones, made of plastic clay materials, strike N50 to N70 with a dip of 50° to 80°NW. The sound blocks are affected by few near-vertical N0 and N90 fractures.

Fracturing analysis at the surface and in the gallery both evidenced the set of fractures oriented N50–70 and dipping 50° to 80°NW, which appears as V-shaped troughs at the surface and as crushed zones in the gallery (see F22, F23 and F25 in Figures 3 and 4a). This major fracture family cut the whole mass and has a predominant role in the deformation processes affecting the accumulation and high motion zones. On the contrary, the fracture set trending N75 and dipping 50°S, which was observed in the gallery, has little expression at the surface except at a local scale. However, these short fractures, parallel to the slope, may have played a role in the mass destabilization, as suggested by Fig. 4a.

5. Geophysical results

5.1. Location of the geophysical profiles

Four 950 m long electrical tomography profiles (labeled ET1 to ET4, Figure 3a) were conducted in the Séchilienne landslide. Profile ET1 is SW–NE oriented (Figure 3a). It starts in the south-western part of the accumulation zone (AZ), runs above the high motion zone (HMZ) and ends in the stable zone (SZ). Profile ET2, oriented N115, starts in the north-western part of the accumulation zone and finishes beneath the HMZ (Figure 3a). Profile ET3 is approximately parallel to ET2 and crosses the Mont Sec head scarp (MHS) and the depletion zone (DZ), ending in the SZ above the AZ (Figure 3a). Finally, Profile ET4 was carried out along the slope (oriented N0°), starting at the Mont Sec scarp foot and extending parallel to the survey gallery (G710) (Figure 3a).

Four 470 m long seismic profiles (labeled ST1 to ST4, Figure 3a) were performed parallel to the electrical ones. ST1 and ST2 are aligned along the ET1 profile, while ST3 and ST4 are acquired along the ET3 profile (Figure 3a). The results of a previously acquired seismic profile (ST5; Meric et al., 2005), running parallel to ET4 with geophone and sources located at the surface and in the survey gallery (G710), have also been used.

5.2. Seismic profiles

The three seismic images obtained after 10 iterations are presented in Fig. 5. For all images, RMS (Root Mean Square) values of the time residuals are lower than 1.7%, implying that each model is coherently consistent with its corresponding data set. Using another initial model (homogeneous with a velocity of 4000 m/s) and adding random noise on the dataset, inversion provided seismic models similar to those shown in Fig. 5 with RMS lower than 1.5%. Along profile ST1–ST2 (Figure 5a), the seismic image shows a superficial low velocity layer (<2000 m/s) with a thickness of about 30 m between 0 and 550 m. This thickness dramatically increases to 100 m over the high motion zone, between 550 and 750 m (Figure 2), highlighting the fracturing induced by the landslide activity. Below 100 m, Vp values increase from 2500 m/s to reach 3500 m/s at 150 m. That latter value characterizes the unweathered and compact micaschists, in agreement with the P-wave velocity measured outside the landslide, on the left bank of the Romanche River by Le Roux et al. (2010). In the SZ, similar high velocities (>3500 m/s) were measured near the surface, suggesting that the compact bedrock is almost outcropping. P-wave velocities appear then to be correlated with the landslide activity and to be able to mark at depth the limit of the disturbed zone. For profile ST3–ST4, the upper part (0–500 m), located over the DZ, exhibits a low velocity zone (<2000 m/s) with a thickness varying from 70 m below the MSH to 150 m at the slope break. These low velocities can be interpreted as the consequence of the damaging effect of the landslide. Below this thick layer, a high velocity gradient is observed with velocities which rapidly reach up to 3500 m/s. The total thickness of the decompressed and fractured zone can thus be estimated below the DZ between 100 and 150 m. In the down part of the profile (500 to 750 m), located in the stable zone, high velocities (>3500 m/s) are measured directly below the surface, suggesting that the bedrock was not deconsolidated.

The P-wave velocity image along profile ST5 (Figure 5c) exhibits a superficial low velocity layer (<2000 m/s) with a thickness varying from 20 to 50 m. Below, the velocity increases heterogeneously to reach more than 3500 m/s at a depth between a few tens of m to 200 m. In particular, a strong lateral velocity gradient (from 2000 m/s to more than 3500 m/s) was observed between abscissa 475 to 525 m, showing that the fracturing degree is not only depth dependent but also varies laterally. A rise of the bedrock (Vp>3500 m/s) was also visibly close to the limit between the AZ and the DZ.

5.3. Electrical profiles

The four electrical images (ET1 to ET4), obtained after 5 iterations, are shown in Fig. 6. The sum of the normalized absolute resistivity residuals divided by the measurement number (absolute error) is lower than 5%. Modifying the starting model and the measured apparent resistivity yielded similar resistivity images, outlining the inversion robustness and stability, except for profile ET3. This issue will be discussed later. For profile ET1, the resistivity section (Figure 6a) shows a shallow resistive layer (thickness <10 m; resistivity >3200 Ω m), probably corresponding to scree deposits covering the slope. Below, significant resistivity contrasts are observed with respect to the different zones. In the stable zone (SZ), low resistivities (100–400 Ω m) were found. These values are in agreement with the measurements made in compact micachists on the left bank of the Romanche River (Le Roux

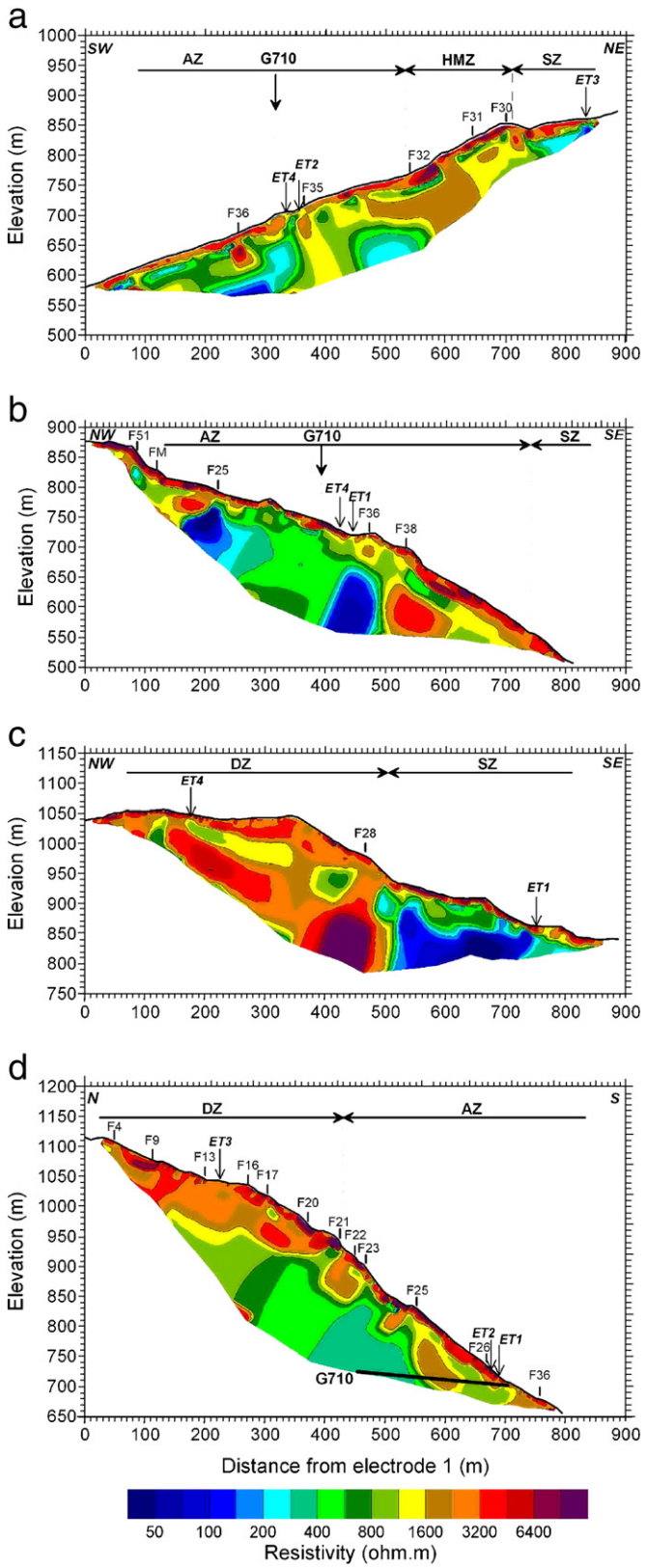

Fig. 6. Electrical tomography sections. (a) Profile ET1, 5 iterations, ABS = 3.6%. (b) Profiles ET2, 5 iterations, ABS = 3.3%. (c) Profile ET3, 5 iterations, ABS = 4.7%. (d) Profile ET4, 5 iterations, ABS = 3.6%. SZ: Stable Zone. HMZ: High Motion Zone. DZ: Depletion Zone. AZ: Accumulation Zone. G710: survey gallery.

et al., 2010). The contact between the SZ and the HMZ (high motion zone) is clearly visible with a dramatic increase in resistivity (1000–2000 Ω m). The thickness of this intensively fractured zone (F30, F31 and F32) reaches at least 100 m. In the accumulation zone (AZ), low resistivities (100–600 Ω m) characterizing compact micaschists were found at about 50 m depth, consistently with the ST1–ST2 seismic tomography. The sound bedrock is overlaid with a higher resistivity layer (800–1600 Ω m), which evidences the fracturing generated by the landslide. A higher near-vertical resistive zone (1200–1800 Ω m) and a local resistive zone (3200–6400 Ω m) is observed at a distance between 350 and 400 m, which are located in the extension of a major fault (F35) visible to the east of the profile. Profile ET2 is entirely located in the accumulation zone (Figure 3). Below shallow resistive scree deposits, the resistivity tomography (Figure 6b) exhibits strong lateral resistivity variations in depth, with a central medium-resistivity part (300–800 Ω m) delineated by two 100 m thick conductive zones (resistivity lower than 200 Ω m), the location of which could fit with cataclasis faults F25 and F36. The lower and upper parts of the profile show higher average resistivity values, suggesting the increase in fracturing near the high motion (F38) and depletion zones (F51 and FM), respectively. Along profile ET4 (Figure 6d), the depletion zone is clearly visible with high resistivity values (1600–6400 Ω m) to 100 m depth, highlighting the intense fracturing under the headscarp (F4, F9, F13, F16, F17, F20 and F21). Below, the rock resistivity is between 200 and 800 Ω m, characterizing low fractured micaschists. At the limit between the depletion and accumulation zones, the thickness of the resistive upper layer sharply decreases, in agreement with the bedrock rise observed along the PS5 seismic profile (Figure 5d). Downward, the resistive layer (>800 Ω m) increases sharply to reach a vertical depth of at least 100 m. The resistivity image ET3 (Figure 6c) exhibits a high lateral resistivity contrast (from a few thousands ohm m to less than 800 Ω m) at the contact between the depletion and the accumulation zones. The thickness of the highly fractured rocks in the depletion zone could reach more than 200 m, in disagreement with the thickness of the low-velocity layer (less than 150 m) measured along the seismic profile ST3–4. As mentioned before, the inversion process for ET3 was found to be unstable (a small change in data yielded different inverted models) and non-unique (different models were obtained for different starting models). In order to get a more reliable solution, we imposed a starting model by fixing the resistivity values with a geometry derived from the seismic image as shown in Fig. 7a (resistivities of the decompressed and sound bedrock are respectively fixed to 5000 and 250 Ω m using the values measured in the other electrical profiles and from previous works for the sound bedrock (Le Roux et al., 2010)). The damping factor of the fixed resistivity areas, which allows the program to change the resistivity of the region, is set to 2.5 (the larger the damping factor weight is used, the smaller is the change that is allowed in the resistivity of the fixed region (Loke, 1998)). The obtained resistivity image (Figure 7b) explains equally well the data (ABS<5%) and is more consistent with the seismic image of Fig. 5b and the crossing electrical image ET4 (Figure 6d). The vertical high resistive zone at the interface between the depletion and accumulation zones could be linked to the influence of the fault F28.

6. Interpretation

Below a few meters thick very low velocity (Vp<1500 m/s) and high resistivity (a few thousands ohm m) layer made of scree deposits covering the slope, the different deformation zones can be characterized through the geophysical investigation, using the P-wave velocity and the electrical resistivity. In the stable zone (SZ), high seismic velocities (Vp>3500 m/s) and low resistivities (<600 Ω m) were measured a few meters below the surface (profile ST1–ST2, Figure 5a, profile ST3–ST4, Figure 5b, profile ET1, Figure 6a, and profile ET3, Figure 7b). These values characterize the micaschists unaffected by the gravitational movement. Notably, Vp of 3500 m/s was proposed as a threshold to differentiate crystalline rocks with poor and fair RQD (Rock Quality Designation) values (Sjøgren et al., 1979; Barton, 2007). On the other hand, considering the inclinometer results with a depth of 80 m for the

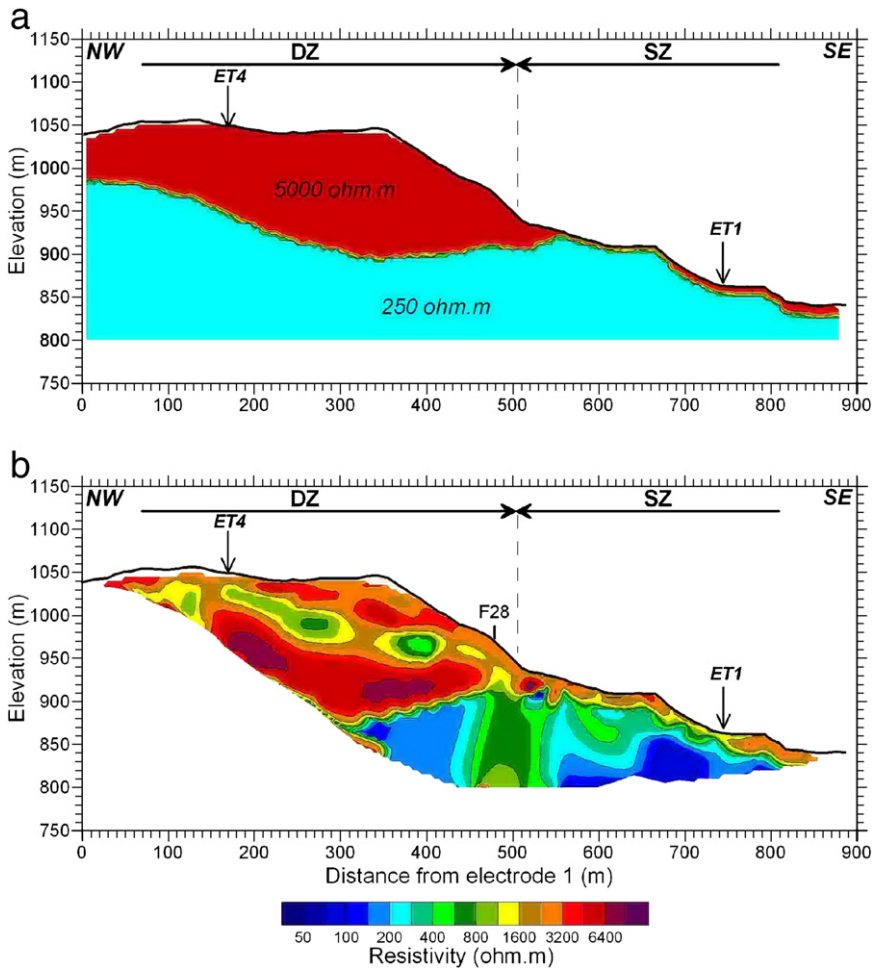

Fig. 7. Electrical tomography sections of profile ET3. (a) Initial resistivity model inferred from seismic interpretation. (b) Resistivity image obtained after 5 iterations, ABS = 3.0%. SZ: Stable Zone. DZ: Depletion Zone.

sliding mass yields a Vp threshold of 3000 m/s, which is of a similar order of magnitude. In the depletion zone (DZ), a strong velocity decrease (Vp<2000 m/s), along with a significant resistivity increase (1600 to 6400 Ω m), was measured to a depth varying between 100 m and 150 m (profile ST3–ST4, Figure 5b; profile ET3, Figure 7b and upper part of profile ET4, Figure 6c). This significant change in geophysical parameters results from the landslide activity which intensively fractured the rocks and favored the presence of air-filled voids. The water has probably no influence on the geophysical parameters, as the table level was found deeper than 130 m in a borehole. Below this layer, the P wave velocities sharply increase to reach 3500 m/s. Associated with a significant decrease in resistivity (200–800 Ω m), these values evidenced the undisturbed micaschists. In the high motion zone (HMZ), those were found at 150 m depth, below thick low-velocity and resistive layers (eastern part of profiles ST1–ST2, Figure 5a and ET1, Figure 6a). Resistivity values (1600–2000 Ω m) are lower than below the depletion zone. In the accumulation zone (AZ), the upper low-velocity (<2000 m/s) and resistive layer is thinner (20 to 50 m; Figure 5a and c) and overlays a layer with intermediate characteristics (Vp around 2000 to 3000 m/s and resistivity lower than 1600 Ω m on average) before reaching the compact bedrock at depths between 100 m and 200 m. This intermediate layer can be laterally heterogeneous (i.e. Figure 5c and Figure 6a, b and d) and exhibits vertical low to very low resistivity zones (50 to 300 Ω m). Moreover, the limit between the AZ and the DZ is characterized by a rise of the high-velocity (>3000 m/s) and low resistivity (<800 Ω m) zone (between abscissa 300 and 500 m along profiles ST5, Figure 5c, and ET4, Figure 6d). The weathered bedrock thus only reaches a thickness of about 50 m in this transition zone. The G710 gallery allows the geophysical parameters to be correlated with the rock conditions (Figure 4a). In the first 140 m, the gallery has encountered intensively fractured rocks (fractured zone, Figure 4a) between the fractures F25 and F26, explaining the high resistivity values (from 800 to 2400 Ω m, Figure 6d) and the relative low P-wave velocity (about 2500 m/s, Figure 5c). In the last 100 m of the gallery, resistivity and P-wave velocity decrease to reach values less than 400 Ω m (Figure 6d) and 2000 m/s (Figure 5c), respectively. This low resistivity and velocity zone correspond to the crushed rocks with clay-filled fractures observed into the gallery (cataclasis zone, Figure 4a) at the crossing with fractures F22 and F23. It then turned out that highly fractured rocks (and the corresponding fractures) could be resistive or conductive as also shown along other resistivity profiles. The resistive property depends on the rock weathering and the fracture filling (air or clay). The very low resistive zones observed on image ET2 probably coincide with the tracing of clay-filled cataclasis zones.

Numerous gradients in velocity or electrical resistivity are either near horizontal or perpendicular to the slope surface. This observation could highlight the role of the near-vertical and parallel-to-the-slope fracture sets on the rock mass sliding and deconsolidation, as sketched in Fig. 4a.

The correlation between geophysical parameters and the rock fracturing degree has been used to derive the rock fissure porosity. Owing to the influence of the fracture filling material on the electrical resistivity, this latter was discarded for computing porosity. The P-wave velocity was considered, applying the Wyllie's law (Eq. 1). We benefited of laboratory measurements made on micaschists before the driving of an investigation gallery on the left bank of the

Table 1
Density, porosity and Vp values measured on micaschist samples (from Effendiantz and Guillot, 2000).

Sample #	Schistosity	Density (.10^3 kg/m^3)	Porosity (%)	V_p (m/s)
1	Non apparent	2.68	0.9	4200
2	Non apparent	2.76	0.9	4890
3	Non apparent	2.69	0.6	4270
4	Slight	2.66	0.7	4390
5	Strong	2.79	1.6	5000
6	Non apparent	2.76	0.8	4490
7	Non apparent	2.73	0.5	5400
8	Non apparent	2.74	0.7	4400
9	Slight	2.67	1.1	4680
10	Non apparent	2.68	1.1	4200
11	Strong	2.76	1.9	5300
12	Non apparent	2.67	1.2	4100
13	Slight	2.68	0.9	4330
14	Non apparent	2.69	0.9	4810
15	Non apparent	2.68	0.5	4620
16	Non apparent	2.84	0.6	6100
17	Non apparent	2.68	0.8	4890
18	Strong	2.82	0.7	5880
19	Slight	2.73	0.8	5020
20	Slight	2.78	0.6	5000
21	Slight	2.79	0.6	5580
Mean		2.73	0.9	4836
Standard deviation		0.05	0.3	551

Romanche river (Effendiantz and Guillot, 2000). Density, porosity and Vp values were measured for 21 rock samples (Table 1) affected, slightly affected or non-affected by schistosity. In the same table are shown the mean and standard deviation values. A P-wave velocity of 4836 m/s was obtained for a porosity of 0.9% and a density of 2.73. The P-wave material velocity (Vp_m) computed from Eq. 1 is 5500 m/s.

Using that value in the Wyllie's law (Eq. 1) we computed the fissure porosity from the measured velocity values, at the scale of the wavelength (a few tens of meters). The corresponding law is shown in Fig. 8a. Although this law is probably not fully adequate, it gives an order of magnitude of the porosity. The porosity images corresponding to the three seismic tomography profiles (Figure 5) are shown in Fig. 8b to d. The velocity in the undisturbed micaschists (3500 m/s) matches a porosity of 3.7%. In the strongly fractured parts of the slope (depletion and high motion zones), porosity can reach values as high as 30%, highlighting the strong damaging effect of the gravitational movement.

From these three seismic images, one previous Vp profile (Meric et al., 2005) and the landslide lateral limits (see Figure 9a for location on the slope DEM), the volume of the mass affected by the Séchilienne landslide was computed, considering a threshold in porosity of 3.7%. Applying the Natural Neighbor gridding method (Watson and Philip, 1987), we reconstruct the landslide geometry (Figure 9b). Subtracting the two DEMs we found a volume of 63×10^6 m^3, a value bracketed by previous estimations (20×10^6 to 100×10^6 m^3, Antoine et al., 1994). Applying two other interpolation methods yields a global volume between 61×10^6 m^3 and 69×10^6 m^3, indicating that the uncertainty resulting from the data scariness is about 10%. Considering a different Vp threshold value of 3000 m/s (corresponding to the interface at 80 m identified by recent inclinometer data, SD-1, Figures 5a and 8b) yields a volume of about 48×10^6 m^3 using the Natural Neighbor method. Considering the different uncertainty sources, a volume of $60\pm10\times10^6$ m^3 could be estimated for the Séchilienne landslide. Notably, this global volume is different from the volume of the HMZ, which was estimated to 3×10^6 m^3. Two topographic cross-sections, drawn through the landslide (located in Figure 9a and b),

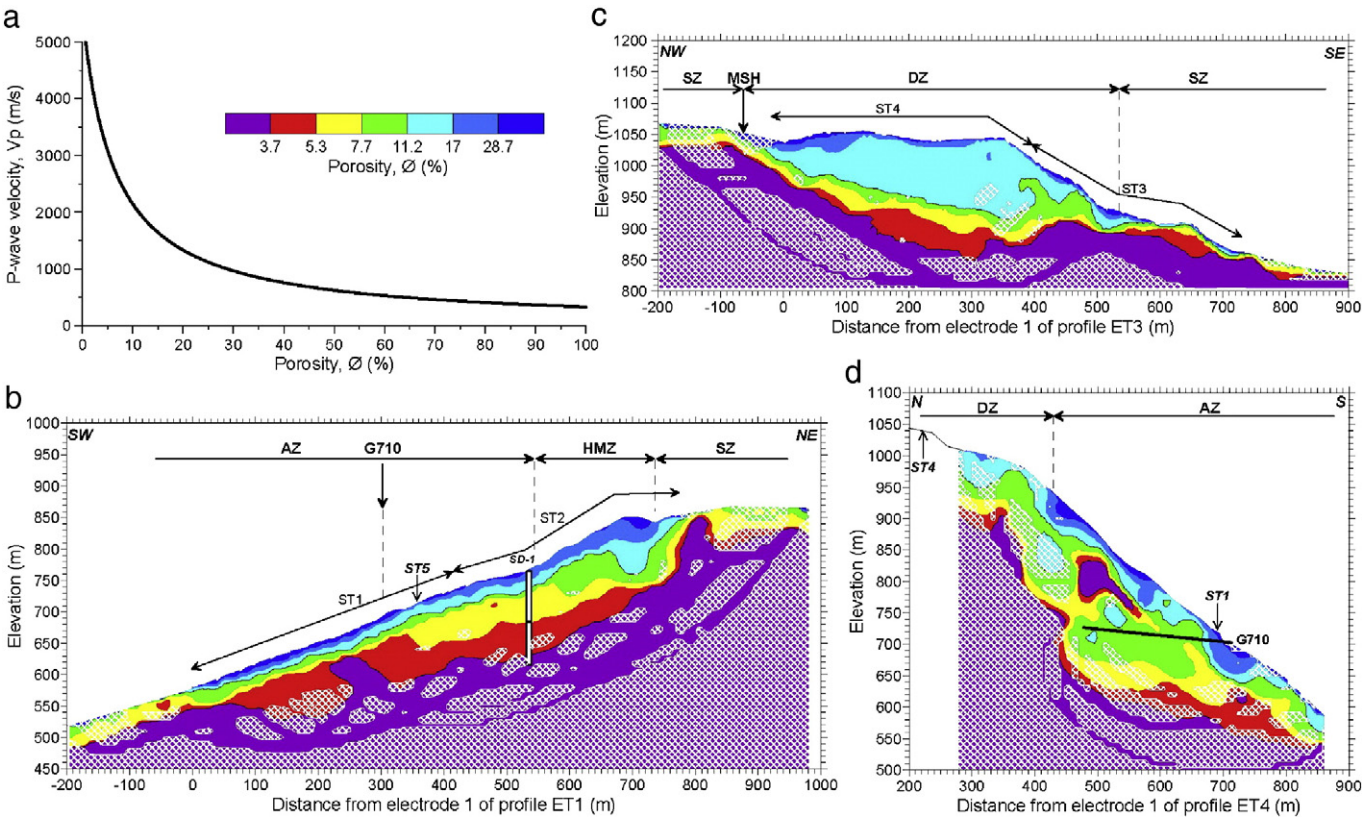

Fig. 8. (a) Vp-porosity empirical law used for the porosity image computation. (b) to (d) Porosity images for profiles ST1–ST2, ST3–ST4 and ST5. White cross-hatching: low ray coverage area. SZ: stable zone. HMZ: high motion zone. MSH: Mont Sec Head scarp. DZ: Depletion Zone. AZ: Accumulation Zone. G710: survey gallery. Borehole SD-1 is located with the limit of detected movements by inclinometer measurements (horizontal line).

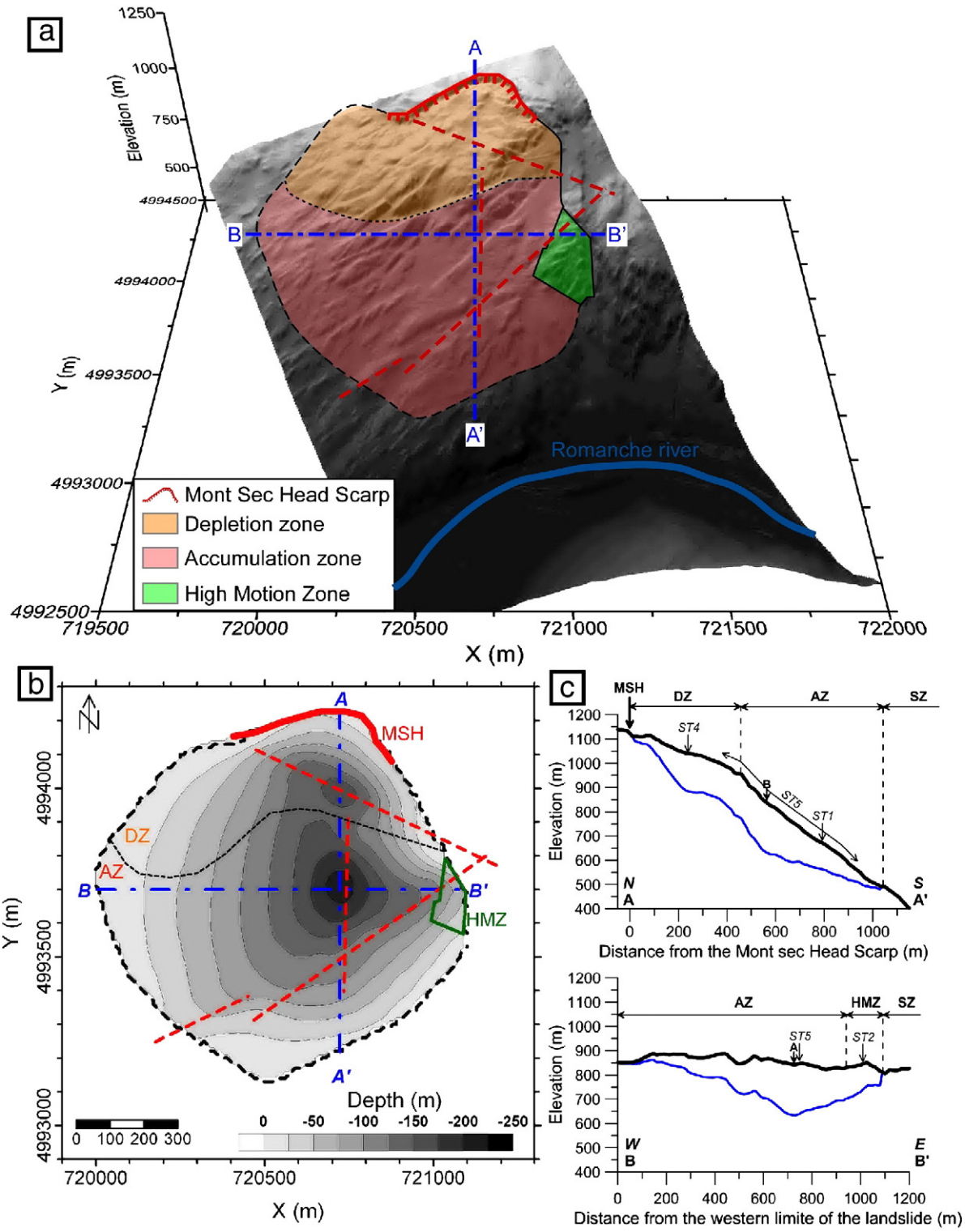

Fig. 9. (a) DEM of the Séchilienne slope with the limits of the landslide zones and the location of the seismic profiles (red dotted lines) and the two cross-sections (blue dotted lines). (b) 2D view of the landslide geometry with the limits of the landslide zones, the location of the seismic profiles (red dotted lines) and the two cross-sections (blue dotted lines). (c) AA′ and BB′ cross-sections with the limit of the mass affected by the landslide, considering a threshold of 3.7% in porosity (blue lines). MSH: Mont Sec Head Scarp. DZ: Depletion Zone. AZ: Accumulation Zone. HMZ: High Motion Zone. SZ: Stable Zone.

delineate the thickness of the moving mass inferred from the threshold in porosity of 3.7% (Figure 9c). They show the lateral asymmetry of the affected volume which is thicker in the central eastern part (cross-section B–B′, Figure 9c) and the rise of the compact bedrock surface at the limit between the DZ and the AZ (cross-section A–A′, Figure 9c). The thickness of the mass affected by the Séchilienne landslide is quite similar in these two zones (about 150 to 200 m). However, the fracturing degree is significantly higher in the DZ and HMZ than in the AZ, as shown by the calculated porosity values (Figure 8).

7. Conclusion

Four long electrical and seismic tomography profiles performed across the Séchilienne landslide allowed the micaschists mass

deconsolidation state to be characterized by P-wave velocity and electrical resistivity values. The zones strongly affected and fractured by the landslide (depletion zone and high motion zone) exhibit low velocity and high resistivity values, resulting from an intense fracturing degree and the presence of air-filled voids as shown the good correspondence between these geophysical parameter variations and the existing geodetic, geomorphic and geological data (investigation gallery and borehole). However, strongly fractured rocks could locally display low resistivity, owing to the presence of vertical cataclasis zones filled with clayey material. This makes resistivity values ambiguous to interpret in terms of fracturing degree and we favored P-wave velocity values for this purpose. Exploiting previous seismic laboratory measurements, we calibrated the Wyllie's experimental law for micaschists and derived the rock mass porosity from P-wave velocity. The volume affected by the landslide was estimated, choosing two possible Vp (or porosity) threshold values for the sound bedrock. The landslide volume was bracketed between 48×10^6 m^3 and 63×10^6 m^3 for a 15% change in Vp (3000–3500 m/s). Although the volume computation appears to be sensitive to the threshold value, this is the first evaluation of the Séchilienne landslide volume, based on deep investigation and not on a mean thickness for the deconsolidated zone. This geophysical study has also contributed to quantify the void percentage created by the landslide in the rock mass, with a maximum value of about 30% in the more deconsolidated zones, as well as the maximum thickness of the affected zone which reaches 150 to 200 m.

Acknowledgments

This work has been funded by the French ministry MEEDDM (Ministère de l'Ecologie, de l'Energie, du Développement Durable et de la Mer) and the ANR project SLAM (Séchilienne Land movement: Multidisciplinary Studies from Hazard assessment to associated risk and consequences). This study was initiated and enriched through numerous discussions with P. Desvarreux (SAGE Company) who unexpectedly died in August 2009. We also thank J.F. Gamond (ISTerre) for his valuable help about the interpretation of geological data.

References

Agliardi, F., Crosta, G., Zanchi, G., 2001. Structural constraints on deep-seated slope deformation kinematics. Eng. Geol. 59, 83–102.
Alfonsi, P., 1997. Relation entre les paramètres hydrogéologiques et la vitesse dans les glissements de terrain. Exemples de La Clapière et de Séchilienne (France). Rev. Fr. Géotech. 79, 3–12.
Antoine, P., Giraud, A., Evrard, H., Rochet, L., 1994. A huge slope movement at Séchilienne, Isère, France. Landslide News 8, 15–18.
Bachmann, D., Bouissou, S., Chemanda, A., 2009. Analysis of massif fracturing during Deep-Seated Gravitational Slope Deformation by physical and numerical modelling. Geomorphology 103 (1), 130–135.
Ballantyne, C.K., 2002. Paraglacial geomorphology. Quatern. Sci. Rev. 21, 1935–2017.
Barféty, J.C., Gidon, M., Montjuvent, G., 1970. Extension et importance des glissements superficiels aux abords méridionaux de Grenoble. Geol. Alpine 46, 17–22.
Barféty, J.C., Bordet, P., Carme, F., Debelmas, J., Meloux, M., Montjuvent, G., Mouterde, R., Sarrot-Reynauld, J., 1972. Notice explicative, carte géologique de la France (1/50.000), feuille Vizille (797). BRGM, Orléans.
Barton, N., 2007. Rock Quality, Seismic Velocity, Attenuation and Anisotropy. Taylor and Francis Group, London, United Kingdom. 741pp.
Brückl, E., Parotidis, M., 2005. Prediction of slope instabilities due to deep-seated gravitational creep. Nat. Hazards Earth Syst. Sci. 5, 155–172.
Chemanda, A., Bouissou, S., Bachmann, D., 2005. 3-D physical modeling of deep-seated landslides: new technique and first results. J. Geophys. Res. 110, F04004. doi:10.1029/2004JF000264.
Claerbout, J.F., Muir, F., 1973. Robust modeling with erratic data. Geophysics 38, 826–844.
Dahlin, T., Zhou, B., 2004. A numerical comparison of 2D resistivity imaging using ten electrode arrays. Geophys. Prospect. 52, 379–398.
Delacourt, C., Allemand, P., Bertier, E., Raucoules, D., Casson, B., Grandjean, P., Pambrun, C., Varel, E., 2007. Remote-sensing techniques for analysing landslide kinematics: a review. Bull. Soc. Geol. Fr. 178 (2), 89–100.
Demanet, D. 2000. Tomographies 2D et 3D à partir de mesures géophysiques en surface et en forage. PhD thesis, Université de Liège, Belgique, 153 pp.
Dines, K., Lyttle, J., 1979. Computerized geophysical tomography. Proc. IEEE 67, 1065–1073.
Dramis, F., Sorriso-Valvo, M., 1994. Deep-seated gravitational slope deformations, related landslides and tectonics. Eng. Geol. 38, 231–243.
Duranthon, J.P., Effendiantz, L., Memier, M., Previtali, I., 2003. Apport des méthodes topographiques et topométriques au suivi du versant rocheux instable des ruines de Séchilienne. Rev. XYZ 94, 31–38.
Durville, J.L., Effendiantz, L., Pothérat, P., Marchesini, P., Bonnard, C., Forlati, F., Scavia, C.A.A., 2004. The Séchilienne landslide. Identification and Mitigation of Large Landslide Risks in Europe. Balkema, Rotterdam, The Netherlands, pp. 253–269.
Effendiantz, L., Guillot, S., 2000. Galerie hydraulique et de reconnaissance géologique de Séchilienne (Isère). Rapport géologique de synthèse, Centre d'études techniques de l'équipement de Lyon. Laboratoire Central des Ponts et Chaussées. 37 p.
Evrard, H., Gouin, T., Benoit, A., Duranthon, J.P., 1990. Séchilienne, risques majeurs d'éboulements en masse; point sur la surveillance du site. Bull. Liaison Ponts Chaussées 165, 7–16.
Giraud, A., Rochet, L., Antoine, P., 1990. Processes of slope failure in cristallophyllian formations. Engineering Geol. 29, 241–253.
Guglielmi, Y., Vengeon, J.M., Bertrand, C., Mudry, J., Follacci, J.P., Giraud, A., 2002. Hydrogeochemistry: an investigation tool to evaluate infiltration into large moving rock masses (case study of La Clapière and Séchilienne alpine landslides). Bull. Eng. Geol. Environ. 61, 311–324.
Guglielmi, Y., Cappa, F., 2010. Regional-scale evolution and large landslides: insights from geomechanical analyses in the Tinée Valley (southern French Alps). Geomorphology 117, 121–129.
Guillot, S., di Paola, S., Ménot, R.P., Ledru, P., Spalla, I., Gosso, G., Schwartz, S., 2010. Suture zones and importance of strike–slip faulting for variscan geodynamic reconstructions of external crystalline massifs of western Alps. Bull. Soc. Geol. Fr. 6, 483–500.
Hagendoorn, J.G., 1959. The Plus–Minus method of interpreting seismic refraction sections. Geophys. Prospect. 7, 158–182.
Heincke, B., Maurer, H.R., Green, A., Willenberg, H., Spillmann, T., Burlini, L., 2006. Characterizing an unstable mountain slope using shallow 2- and 3-D seismic tomography. Geophysics 71 (6), B241–B256.
Heincke, B., Günther, T., Dalsegg, E., Rønning, J.S., Ganerød, G.V., Elvebakk, H., 2010. Combined three-dimensional electric and seismic tomography study on the knes rockslide in western Norway. J. Appl. Geophys. 70 (4), 292–306.
Helmstetter, A., Garambois, S., 2010. Seismic monitoring of Séchilienne Rockslide (French Alps): analysis of seismic signals and their correlation with rainfalls. J. Geophys. Res. 115, F03016. doi:10.1029/2009JF001532.
Jongmans, D., Garambois, S., 2007. Geophysical investigation of landslides: a review. Bull. Soc. Geol. Fr. 178 (2), 101–112.
Kasperski, J., Pothérat, P., Duranthon, J.P., 2010. Le mouvement de versant de Séchilienne: point sur l'activité du phénomène. Proceedings of the Rock Slope Stability symposium, Paris. 24–25 November 2010, 13 p.
Le Roux, O., Schwartz, S., Gamond, J.F., Jongmans, D., Bourlès, D., Braucher, R., Mahaney, W., Carcaillet, J., Leanni, L., 2009. CRE dating on the head scarp of a major landslide (Séchilienne, French Alps), age constraints on Holocene kinematics. Earth Planet. Sci. Lett. 280, 236–245. doi:10.1016/j.epsl.2009.01.034.
Le Roux, O., 2009. Caractérisation de l'évolution géomorphologique de la basse vallée de la Romanche en relation avec les instabilités gravitaires de ses versants rocheux, contraintes morphologiques, géophysiques et géochronologiques. Thèse de doctorat de l'université Joseph Fourier, Grenoble. 321 pp.
Le Roux, O., Schwartz, S., Gamond, J.F., Jongmans, D., Tricart, P., Sebrier, M., 2010. Interaction between tectonic and erosion processes on the morphogenesis of an alpine valley: geological and geophysical investigations in the lower Romanche valley (Belledonne massif, western Alps). Int. J. Earth Sci. 99, 427–441. doi:10.1007/s00531-008-0393-1.
Le Roux, O., 2010. Caractérisation de l'évolution géomorphologique de la basse vallée de la Romanche en relation avec les instabilités gravitaires de ses versants rocheux. Bull. Engineering Geol. Environment. doi:10.1007/s10064-010-0325-8.
Lebourg, T., Binet, S., Tric, E., Jomard, H., El Bedoui, S., 2005. Geophysical survey to estimate the 3D sliding surface and the 4D evolution of the water pressure on part of a deep seated landslide. Terra Nova 17, 399–406.
Leucci, G., De Giorgi, L., 2006. Experimental studies on the effects of fracture on the P and S wave velocity propagation in sedimentary rock ("calcarenite del Salento"). Eng. Geol. 84, 130–142.
Loke, M.H., Barker, R.D., 1996. Least-squares deconvolution of apparent resistivity pseudosections. Geophysics 60 (6), 1682–1690.
Loke, M.H., 1998. Res2dInv, Rapid 2D Resistivity and IP inversion using the least squares method — user's manual.
Martinod, J., Roux, L., Gamond, J.F., Glot, J.P., 2001. Present-day deformation of the Belledonne Massif (External Alps, France): comparison triangulation-GPS. Bull. Soc. Geol. Fr. 172, 713–721.
Mavko, G., Mukerji, T., Dvorkin, J., 1998. The Rock Physics Handbook. Cambridge University Press. 340 pp.
Ménot, R.P., 1988. An overview of the geology of the Belledonne massif (external crystalline massifs of Western Alps). Swiss Bull. Mineralog. Petrol. 70, 33–53.
Meric, O., Garambois, S., Jongmans, D., Wathelet, M., Chatelain, J.L., Vengeon, J.M., 2005. Application of geophysical methods for the investigation of the large gravitational mass movement of Séchilienne (France). Can. Geotech. J. 42, 1105–1115. doi:10.1139/t05-034.
Metternicht, G., Hurni, L., Gogu, R., 2005. Remote sensing of landslides: An analysis of the potential contribution to geospatial systems for hazard assessment in mountainous environments. Remote Sens. Environ. 98, 284–303.
Montjuvent, G., Winistorfer, J., 1980. Glaciations quaternaires dans les Alpes franco-suisses et leur piedmont. Geol. Alpine 56, 251–282.
Petley, D.N., Mantovani, F., Bulmer, M.H., Zannoni, A., 2005. The use of surface monitoring data for the interpretation of landslide movement patterns. Geomorphology 66, 133–147.

Potherat, P., Alfonsi, P., 2001. Les mouvements de versant de Séchilienne (Isère). Prise 'compte' héritage structural leur simulation numérique. Rev. Fr. Géotechnique. 95, 117–131.
Reynolds, J.M., 1997. An Introduction to Applied and Environmental Geophysics. John Wiley and Sons Ltd, Chichester. 796 pp.
Rochet, L., Giraud, A., Antoine, P., Evrard, H., 1994. La déformation du versant Sud du Mont sec dans le secteur des ruines de Séchilienne (Isère, France). Bull. 'Association Int. Géol.' Ingénieur 50, 75–87.
Sanchez, G., Rolland, Y., Corsini, M., Braucher, R., Bourlès, D., 2010. Cosmic ray exposure dating of active faulting and landslides in the SW Alps: relationships between tectonics, slope instabilities and climate changes. Geomorphology 117, 1–13.
Sjøgren, B., Øfsthus, A., Sandberg, J., 1979. Seismic classification of rock mass qualities. Geophys. Prospect. 27, 409–442.
Telford, W.M., Geldart, L.P., Sheriff, R.E., 1990. Applied Geophysics, second edition. Cambridge University Press. 751 pp.
Thouvenot, F., Frechet, J., Jenatton, L., Gamond, J.F., 2003. The Belledonne Border Fault: identification of an active seismic strike–slip fault in the western Alps. Geophys. J. Int. 155, 174–192.
Vengeon, J.M., 1998. Deformation et rupture des versants en terrain métamorphique anisotrope. Apport de l'étude des ruines de Séchilienne. PhD thesis, Université Grenoble I, France, 186 pp.
Vengeon, J.M., Giraud, A., Antoine, P., Rochet, L., 1999. Analysis of the deformation and toppling of rock slopes in crystallophyllian terrain. Can. Geotech. J. 36, 1123–1136.
Watson, D.F., Philip, G.M., 1987. Neighborhood based interpolation. Geobyte 2, 12–16.
Wyllie, M.R.J., Gregory, A.R., Gardner, L.W., 1956. Elastic wave velocities in heterogeneous and porous media. Geophysics 21 (1), 41–70.